Robotica (2018) volume 36, pp. 333–352. © Cambridge University Press 2017
doi:10.1017/S0263574717000418

Efficient motion generation for a six-legged robot walking on irregular terrain via integrated foothold selection and optimization-based whole-body planning

Yuan Tian and Feng Gao*

State Key Laboratory of Mechanical System and Vibration, Shanghai Jiao Tong University, 200240 Shanghai, P.R. China. E-mail: tianyuan_123abc@sjtu.edu.cn

(Accepted September 30, 2017. First published online: November 6, 2017)

SUMMARY

In this paper, an efficient motion planning method is proposed for a six-legged robot walking on irregular terrain. The method provides the robot with fast-generated free-gait motions to traverse the terrain with medium irregularities. We first of all introduce our six-legged robot with legs in parallel mechanism. After that, we decompose the motion planning problem into two main steps: first is the foothold selection based on a local footstep cost map, in which both terrain features and the robot mobility are considered; second is a whole-body configuration planner which casts the problem into a general convex optimization problem. Such decomposition reduces the complexity of the motion planning problem. Along with the two-step planner, discussions are also given in terms of the robot-environmental relationship, convexity of constraints and robot rotation integration. Both simulations and experiments are carried out on typical irregular terrains. The results demonstrate effectiveness of the planning method.

KEYWORDS: six-legged robot, motion planning, foothold selection, optimization

1. Introduction

Stable locomotion on irregular terrain is a common and essential issue in legged robotics. Unlike on structured or flat terrains where a set of simple gaits and motions could sufficiently adapt to the terrain feature, more autonomy of the robot is required on irregular terrains. Such autonomous behaviors often consist of the terrain feature acquisition, modeling, foothold selection and finally the continuous motion generation. These are necessary steps in an accurate planning scheme, yet it is challenging to integrate these aspects and effectively generate feasible motions.

First of all, for locomotion on unknown terrains, sensory information such as vision and forces are essential to acquiring terrain features. There are also light, compliant robots that are biologically inspired and highly dynamic such as Rhex[1] which may require less knowledge about environments and less accurate trajectories. Yet in this paper, we would like to discuss within the accurate planning scheme which to our knowledge is generally applied by most legged robots and depends less on specific mechanical designs.

On irregular terrains, foothold selection is one of the primary issues of motion planning once the terrain information is obtained or assumed known. The selection approach has been considered earlier for humanoid robots. Kuffner Jr, *et al.*[2] proposed a dynamic programming approach to realize biped-robot moving in obstacle-clustered environments. Judged with a discrete set of plausible motions, the biped-robot determined to whether step on or step over an obstacle. A more humanistic approach to traverse obstacles with different intuitive strategies was adopted by Ayaz, *et al.*[3] However, only the flat terrains with clustered obstacles were discussed in their studies. Deits and

* Corresponding author. E-mail: gaofengsjtu@gmail.com

Tedrake[4] investigated the application of mixed-integer convex optimization for a humanoid robot in unstructured environments and achieved stable walking motions. For quadruped robots, researches on the Littledog platform have been showing good potential. Kalakrishnan, *et al.*[5] proposed the terrain template learning algorithm, based on which an optimal foothold with the maximum reward could be found. In addition, anytime repairing A* (ARA*) is applied for scenarios of kinematically challenging terrains. Zucker, *et al.*[6] employed an expert system to compute the terrain cost and the body pose cost functions. Kolter and Ng[7] also adopted the apprenticeship learning method to compute terrain cost from expert demonstration. During training, numbers of features are involved including information from the elevation map, potential collisions, the form of the support triangle, etc. A box search near the desired position was carried out to find the optimal foothold. It is not hard to notice that learning-based methods were frequently employed. These methods successfully resolved the problem with hierarchical and reliable strategies, yet they required both offline and online computation, with terrain templates or similar terrain features accessible before the walking began. As a matter of fact, this is not common in real world locomotion tasks. In most situations, only a limited range of terrain information can be perceived, therefore referring to the aforementioned researches, an online fast-generated local cost map as well as a simple searching process would be a suitable alternative. For the six-legged robot, an obvious difference is the gait pattern applied. The sequential creeping gait and footholds was early investigated by Ozguner, *et al.*[8] with preview information while the hexapod crossed over rough terrain. However, as a natural advantage of the hexapod, the tripod gait has been mostly adopted, which requires foothold selection for three swing legs at a time. It is more complex than the sequential creeping gait since the variable dimension at least triples up and the related features as well. In such case, the expert system employed on the quadruped may not be so effective, because it is already quite obscure to demonstrate multiple optimal footholds by the expert; moreover, the complexity would greatly increase during training. On the other hand, promising results were achieved on the hexapod Messor.[9] A real-time mapping method as well as foothold selection using 2D laser scanner data was proposed. A dynamics-embedded simulator capable of detecting collisions and modeling frictions was deployed to simulate slippage, helping the swing leg make real-world decisions according to the geometric properties of the terrain including concavity and sloppiness. Leg kinematic margins were guaranteed by a body posture optimizer for stance legs and a steepest descent searching for swing legs.[10,11]

Good foothold selection strategies can help a robot maintain walking steadiness, while for continuous motions, the robot still need proper planning to achieve stability, avoid collisions and kinematic deadlocks. Classic approaches for the motion planning problem are variations of several general approaches, namely roadmap, cell decomposition, potential fields and mathematical programming. These approaches can resolve most motion planning problems yet may encounter high time complexity in certain situations;[12] heuristic algorithms such as Probabilistic Roadmaps[13] and Rapidly exploring Random Trees[14] were developed and proved to possess high efficiency yet the motion optimality needs further consideration. For legged robots, motion planning are embodied in two aspects: one is the path generation, the other is the robot motion during steps. In this paper, we focus the discussions on the latter one. Related MP problems have been studied applying various methods. The six-legged lunar robot Athlete[15] applied a variant of the Probabilistic Roadmap approach to generate transitions between robot stances. The constraints of the configuration space was investigated. A stance graph was employed to describe the connectivity between stances. Ratliff, *et al.*[16] proposed novel gradient optimization techniques (CHOMP) for trajectory planning of the LittleDog robot over obstacles. For each footstep, with a given initial trajectory, the CHOMP ran as the coordinate descent switching between the trunk trajectory and the swing leg trajectory, and eventually a collision-free trajectory could be obtained. Also on LittleDog, Kolter and Ng[17] presented a convex optimization based approach to optimize cubic spline trajectories of the swing leg and the body separately by setting convex constraints and smoothness objectives. A mixed-integer quadratically constrained quadratic programming (MIQCP) was employed by Deits and Tedrake[4] to deal with non-convex constraints of the biped-robot motion with promising computational performance. The common purpose of the aforementioned studies is to figure out the relationship between robot motions and various constraints, and finally seek for feasible transitions between a starting configuration and a goal configuration. For the tripod gait motion planning of a six-legged robot, difficulties exist in solving the coupling motion problem of the body and more than one single swing leg. Therefore, a series of intermediate configurations of the robot are necessary. Moreover, considering also the algorithm complexity, especially when an online planner is needed, simple handling procedures are encouraged.

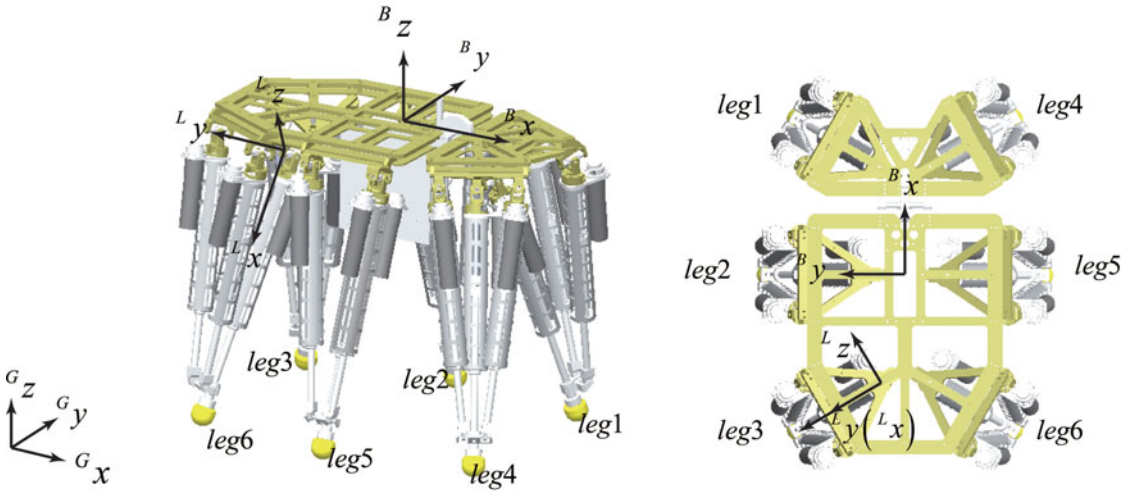

Fig. 1. Different coordinate systems and the sequence of legs.

In this paper, we present a fast foothold selection method based on locally generated footstep cost and optimization-based whole-body configuration planning, both developed on our six-legged robot. First of all, our six-legged robot with legs in parallel mechanism is introduced, including its kinematics and system composition. After that, the terrain modeling is conducted. A local footstep cost map is given through the analysis on both the footstep feasibility cost and the cost related to the robot-environmental relationship. Once proper footholds are given for the swing legs, the planning for the whole step is possible with a simple terrain reference generated from the local terrain feature. Upon the terrain reference, an integrated convex optimization-based method is employed to eventually compute the featured whole-body configurations within the step. Convex constraints are formulized concerning the strict limitations of the robot stability, kinematics and collisions. Our two-step planner has the advantage of fast online generation of feasible motions. At last, simulations and experiments are carried out on irregular terrains to prove the effectiveness of the approach.

2. System Overview

2.1. The six-legged robot

The six legs of the robot are symmetrically distributed w.r.t. the x–z plane of the robot body (Fig. 1). There are three types of coordinate systems (CS), namely the ground reference CS, the robot body CS and the robot leg CS. In the following of the paper, all motion variables without the superscript on the left are assumed to be w.r.t. the ground reference CS. The robot upper body part is of dimension 1070 mm*660 mm, and the overall configuration is of dimension 1330 mm*730 mm*850 mm in its standstill status. The robot weighs around 260 kg in total, in which the robot body weight is around 200 kg. Payload of the robot can reach as high as 500 kg thanks to its legs in parallel mechanism.

Each leg contains three sub-chains in parallel, actuated by three servo motors via transmission of the lead screw. The leg mechanism is 2UPS-1UP, illustrated in Fig. 2, leading to three translational degrees of freedom of the foot. Each foot has a hemispherical rubber foot tip to increase friction and reduce slippery. The inverse kinematics (IK) of the leg is given w.r.t. the corresponding leg CS:

$$\text{screw}_{\boldsymbol{d}_i} = \mathbf{IK}(L_{i_{\boldsymbol{p}_{f_i}}}) \tag{1}$$

where $L_{i_{\boldsymbol{p}_{f_i}}}$ is the *ith* foot tip position w.r.t. the *ith* leg CS and $\text{screw}_{\boldsymbol{d}_i}$ represents three screw lengths of the *ith* leg. The parallel leg mechanism benefits from having a close-formed explicit IK solution, which facilitates the real-time computation. Detailed resolution was elaborated in previous research.[18] For each leg, the screw lengths $\text{screw}_{\boldsymbol{d}_i}$ have corresponding upper and lower bounds due to mechanical

https://doi.org/10.1017/S0263574717000418 Published online by Cambridge University Press

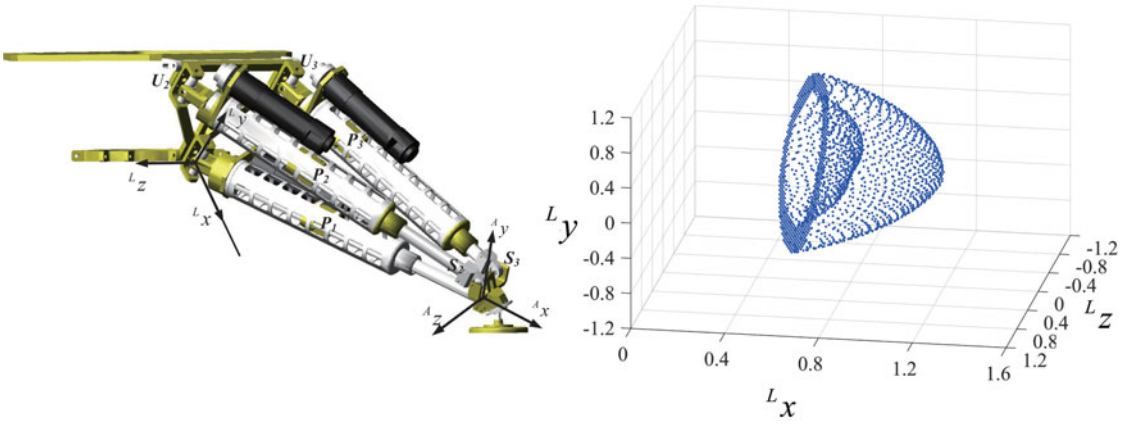

Fig. 2. Leg in parallel mechanism and its workspace w.r.t. the leg coordinate system.

constraints and thus give a solid and bounded workspace shown in Fig. 2. The foot tip kinematic accuracy is within 5 mm.

The leg IK w.r.t. the ground CS is:

$$\text{screw}_{\boldsymbol{d}_i} = \mathbf{IK}\left({}^{L_i}_{B}\boldsymbol{T}\,{}^{B}_{G}\boldsymbol{T}\begin{bmatrix}{}^{G}\boldsymbol{p}_{f_i}\\ 1\end{bmatrix}\right) \tag{2}$$

$$\text{where } {}^{B}_{G}\boldsymbol{T} = \begin{bmatrix}\boldsymbol{R}^{-1}\left({}^{G}\boldsymbol{\psi}_b\right) & -\boldsymbol{R}^{-1}\left({}^{G}\boldsymbol{\psi}_b\right)\cdot{}^{G}\boldsymbol{p}_b\\ 0_{(1\times 3)} & 1\end{bmatrix} \tag{3}$$

$$\text{and } {}^{L_i}_{B}\boldsymbol{T} = \begin{bmatrix}\boldsymbol{R}^{-1}\left({}^{B}\boldsymbol{\psi}_{h_i}\right) & -\boldsymbol{R}^{-1}\left({}^{B}\boldsymbol{\psi}_{h_i}\right)\cdot{}^{B}\boldsymbol{p}_{h_i}\\ 0_{(1\times 3)} & 1\end{bmatrix} \tag{4}$$

are homogenous transformation matrices between different CSs. ${}^{G}\boldsymbol{p}_b$ and ${}^{G}\boldsymbol{\psi}_b$ are position and orientation of the body w.r.t. the ground CS. ${}^{B}\boldsymbol{p}_{h_i}$ and ${}^{B}\boldsymbol{\psi}_{h_i}$ are positon and orientation of the *ith* hip w.r.t. the body CS and they are predetermined according to the robot structure.

The parallel mechanism leads to better payload and actuation fault tolerance, so that the robot could be applied to various tasks with considerable payload, even with some malfunctioned motors.[19] Yet, the workspace of the robot leg in parallel mechanism is limited compared to serially actuated counterparts.[20] Although the robot could walk without difficulty on flat terrains, deadlocks frequently occur when it tries to traverse terrains with non-negligible obstacles without optimizing the motion. This is one essential reason why we propose our two-step planner.

For the control system, we employ a Linux OS with a cross-compiled Xenomai real-time core. The control frequency is 1 KHz. Legs are actuated by a total of eighteen 400 W brushless servo motors. The Lithium battery as the power supply is mounted on the body of the robot. Onboard sensory systems are also applied, including an IMU unit, a six degree-of-freedom force sensor on the body and a Kinect 3D stereo vision system from which raw vision point cloud is generated. In terms of visionary perception, the following terms are necessary for the development of this paper:

(a) A fast-generated elevation map of the terrain with proper accuracy and vision range.
(b) A reasonable and traversable reference path over the terrain.

The first term is fundamental and its vision range should be at least sufficient to plan the next period of the robot motion. In our system, the vision system generates an elevation map of local objects on sight with a frequency of 10 Hz and the vision range is around 1.5 m × 1.5 m with a resolution of 0.025 m × 0.025 m. The elevation accuracy is within 2 cm. The second term could be interperated as excluding non-traversable terrain and large obstacles along the path. The above terms play as the prerequisites of the planner.

https://doi.org/10.1017/S0263574717000418 Published online by Cambridge University Press

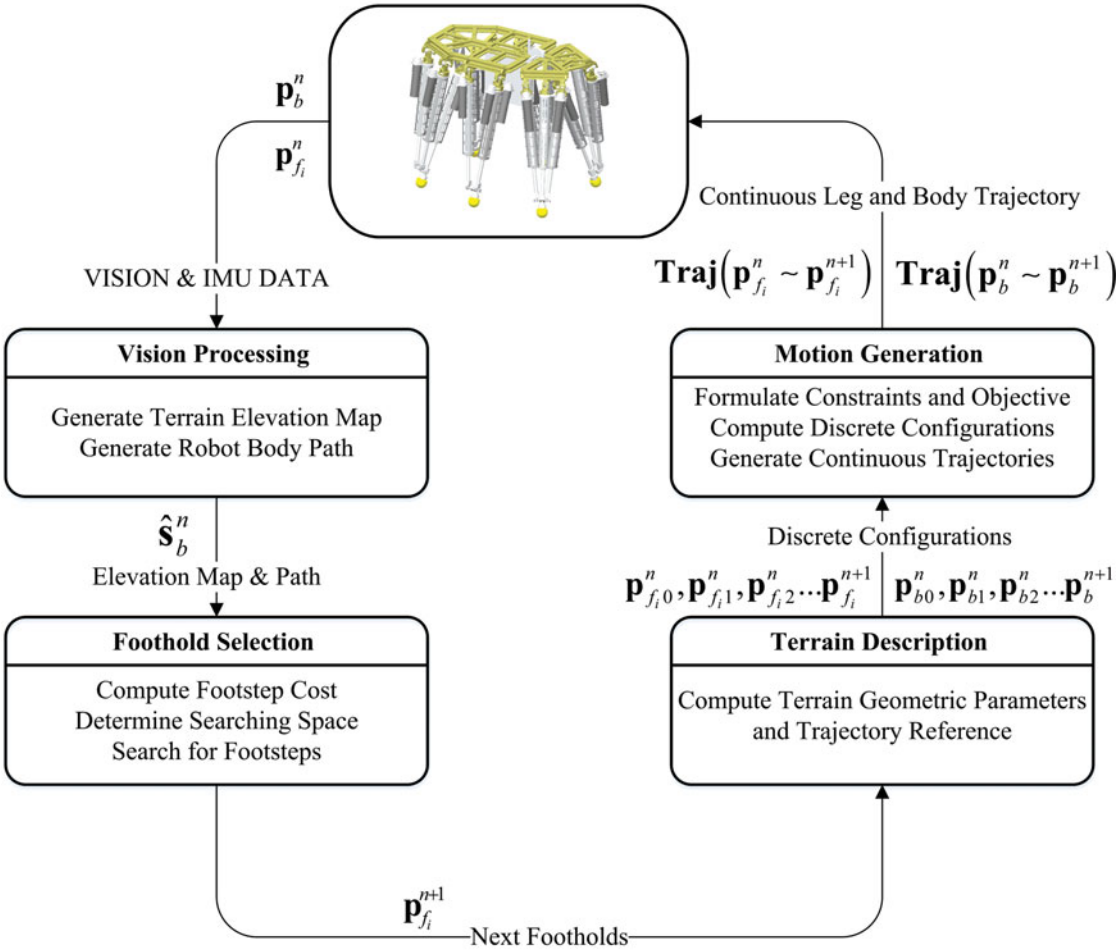

Fig. 3. The planner overview. $\hat{\boldsymbol{s}}_b^n$ represents the estimated body displacement. $\boldsymbol{p}_{f_i}^{n+1}$ is the next chosen foothold for each swing leg *i*. $\boldsymbol{p}_{f_i0}^n, \boldsymbol{p}_{f_i1}^n, \boldsymbol{p}_{f_i2} \ldots \boldsymbol{p}_{f_i}^{n+1}$ and $\boldsymbol{p}_{b0}^n, \boldsymbol{p}_{b1}^n, \boldsymbol{p}_{b2} \ldots \boldsymbol{p}_b^{n+1}$ are leg and body motion waypoints belonging to intermediate configurations of the robot. Traj($\boldsymbol{p}_{f_i}^n \sim \boldsymbol{p}_{f_i}^{n+1}$) and Traj($\boldsymbol{p}_b^n \sim \boldsymbol{p}_b^{n+1}$) are final robot trajectories for the step.

2.2. Planner overview

The tripod gait is employed as the most frequently used gait of the six-legged robot. In addition, we describe the period between the two stances of six legs as one step. The body and the legs displacements w.r.t. the ground CS during the *nth* step are:

$$\boldsymbol{p}_b^{n+1} = \boldsymbol{p}_b^n + \boldsymbol{s}_b^n \tag{5}$$

$$\boldsymbol{p}_{f_i}^{n+1} = \boldsymbol{p}_{f_i}^n + \boldsymbol{s}_{f_i}^n, \quad \text{for } i \in 1 \sim 6 \tag{6}$$

where $\boldsymbol{s}_b^n$ represents the body displacement and $\boldsymbol{s}_{f_i}^n$ represents the leg displacement, being zero for any stance leg. During one step period, motion of the legs and the body need to be planned as a function of time. Other than that, features of the terrain should be equally concerned as solid constraints. Other conditions include the robot stability, the kinematic reachability, etc. All factors are relevant, but we try to resolve the problem by studying sub-problems in a decoupled and sequential manner. Fig. 3 illustrates the planning steps.

We decouple the foothold selection from the continuous motion planning because the foothold selection depends on both the terrain information and the robot mobility. It deals with the robot-environmental relationship to finally obtain discrete solutions while the rest of the motion planning is resolved in a continuous scheme. The CHOMP approach also decomposes the problem into foothold

https://doi.org/10.1017/S0263574717000418 Published online by Cambridge University Press

selection and footstep motion planning in order to decrease the problem complexity.[16] The decoupled two-step planner could reduce the complexity of the problem and still stay effective.

3. Foothold Selection

This section presents the first part of the planning strategy, an integrated terrain modeling method to convert reliable environmental information into useful assessment to eventually determine proper footholds for the swing legs.

3.1. Footstep cost

Apart from the basic information acquired form the vision system, it is specifically required by the multi-legged robot to be able to determine feasible footholds. The terrain type considered in this paper is the traversable terrain, since we assume that non-traversable obstacles have already been effectively avoided by the vision navigation system. This is why we reasonably assume that for each foot, referring to the path of the robot body, its foothold selection from the current configuration could be achieved by an optimal search in the desirable area. The definition of the searching area will be given in Section 3.2. Before that, a footstep cost function is provided.

To propose a footstep cost function, the properness of a footstep is firstly evaluated. A proper footstep leads to two advantages. The first is to support the robot motion with sufficient force. The second is to enable the robot to be redundant enough to generate a series of motion that meets the kinematic and environmental constraints. Therefore, we discuss the foothold selection in two aspects. One is the independent analysis of the terrain feasibility as a supportable foothold. The other is the analysis based on the robot-terrain relationship.

3.1.1. Foothold feasibility based on local flatness. Slippage and instability occurs when a leg of the robot land on the bad foothold for it may not offer sufficient friction or support force for the robot. Such terrain features include edges, steer slopes, etc. The local flatness around a certain terrain position could effectively reflect its feasibility as the foothold. The numerical value is assigned as follows to express the flatness, which is the elevation variance of the adjacent area around the grid point (x, y).

$$F_{(x,y)} = \sum\nolimits_{(i,j)\in B_f(x,y)} \left(\left(z_{(i,j)} - E\left(z_{(i,j)} \right) \right)^2 \right) \tag{7}$$

in which the coordinate variables i and j are integers that represent grid numbers and are defined in the ground CS. $E(.)$ represents the expectation or mean value, which mathematically leads to the expression $F_{(x,y)}$ as the elevation variance. $B_f(x, y)$ is the box chosen for grid point (x, y) in terms of foothold feasibility. The box-shaped generalization area around a grid point is defined as:

$$B\left(i, j\right) | [x_-, x_+, y_-, y_+] = \cup (a, b), \quad \text{for } \forall a \in [i - x_-, i + x_+], b \in [j - y_-, j + y_+] \tag{8}$$

which is a 2D box of discrete points of the terrain grid.

The box dimension of B_f should be large enough to cover the size of a foot tip of diameter d_f and yet not so large that the cost function would over generalize the terrain feature. Therefore, we adapt the box parameter of B_f as:

$$\left[x_{f-}, x_{f+}, y_{f-}, y_{f+} \right] = \left[\frac{d_f}{r}, \frac{d_f}{r}, \frac{d_f}{r}, \frac{d_f}{r} \right] \tag{9}$$

in which the operator $\lceil \cdot \rceil$ means rounding up to an integer and r is the resolution of the terrain grid. After that we adopt a two-valued feasibility cost function for each point of the terrain grid. In other words, we assume that all feasible footholds can be trusted as being capable to support the robot, yet infeasible footholds are simply not regarded for the subsequent foothold evaluation.

$$J_{(x,y)}^{\text{feasibility}} = \begin{cases} 0, & \text{if } F_{(x,y)} < F_{\text{threshold}} \\ +\infty, & \text{if } F_{(x,y)} \geq F_{\text{threshold}} \end{cases} \tag{10}$$

which categorizes feasible and infeasible footholds using $F_{\text{threshold}}$ as the threshold value.

https://doi.org/10.1017/S0263574717000418 Published online by Cambridge University Press

3.1.2. Concave corner cost. We believe that footholds should be selected such that the robot could achieve relatively redundant motion in the adjacent pose space. The discussion must involve solid constraints from terrains. According to experimental experiences, when the robot foothold is selected near a concave corner, the robot body redundancy would be greatly limited. It is important to mention that the concavity studied here is not the small one proposed by Belter, *et al.*[21] which would make a good foothold, but the larger one that interferes the leg motion. Moreover, on our robot, the rubber foot tip has large friction coefficient on rigid ground, therefore the small benefit of the small concavity is not considered.

The concave corner would limit the continuous leg motion thus the robot corresponding configurations. Collisions would occur between the terrain and a certain robot part, especially shins. The leg is therefore "trapped" in some way. To describe such cost, two factors are involved, one is the absolute elevation value of the foothold candidate, and the other is the elevation of the neighboring terrain around it. We define the concave corner cost of the grid point (x, y) as follows:

$$J_{(x,y)}^{\text{concavity}} = \sum\nolimits_{(i,j)\in B_c(x,y)} D_{(i,j)} \tag{11}$$

in which $D_{(i,j)}$ is the cost of a grid point adjacent to (x, y) within $B_c(x, y)$:

$$D_{(i,j)} = \begin{cases} 0, & \text{if } z_{(i,j)} \le z_{(x,y)} \\ \frac{\left\| z_{(x,y)} - z_{(i,j)} \right\|^2}{i^2+j^2}, & \text{if } z_{(i,j)} > z_{(x,y)} \\ 0, & \text{if } i = j = 0 \end{cases} \tag{12}$$

and the neighboring area B_c is of dimension,

$$\left[x_{c-}, x_{c+}, y_{c-}, y_{c+}\right] = \left[\left\lceil \frac{d_x}{r} \right\rceil, \left\lceil \frac{d_x}{r} \right\rceil, \left\lceil \frac{d_y}{r} \right\rceil, \left\lceil \frac{d_y}{r} \right\rceil\right] \tag{13}$$

Note that, if the terrain is open wide and flat, even it is relatively low, it barely costs the robot leg to choose it as the foothold, so that the neighboring area should have a well-attended limitation. d_x and d_y are dimensions of B_c we choose in order to leave a proper margin for the foothold to avoid potential collision during the continuous motion. They are related to the robot dimension and the mobility of legs. For the step of our robot, we adapt d_x as 15 cm and d_y as 5 cm.

The overall footstep cost $J_{(x,y)}$ is the summation of the foothold feasibility cost and the concavity cost. The weights are not necessary because the foothold feasibility cost is either zero or infinity.

$$J_{(x,y)} = J_{(x,y)}^{\text{feasibility}} + J_{(x,y)}^{\text{concavity}} \tag{14}$$

In this section, we decouple the foothold selection procedure into selecting feasible footholds and then considering the cost related to the robot structure. A feasible foothold with a minimum local cost is the optimal choice for a swing leg to touch down. Now it only leaves a proper searching range to determine.

3.2. Foothold searching

Once the footstep cost function is determined, the optimal search procedure could be executed. Yet, an improper searching range could lead to unsatisfying outcomes. As previously introduced, the planner schedules the next footholds for swing legs from the latest stance configuration. The tripod gait requires the supporting triangle continuously, it becomes more complex than selecting a single swing leg foothold due to the coupled motion of the swing legs. Therefore, we propose the approach concerning the following terms to determine the searching space:

(a) The desirable foothold positions as the searching centers.
(b) The searching range determined by a proper adjacent area around each searching center.

To determine the ideal foothold positions of the three swing legs, we propose the Robot Configuration with Maximum Kinematic Margin (RCMKM). The kinematic margin is defined as

https://doi.org/10.1017/S0263574717000418 Published online by Cambridge University Press

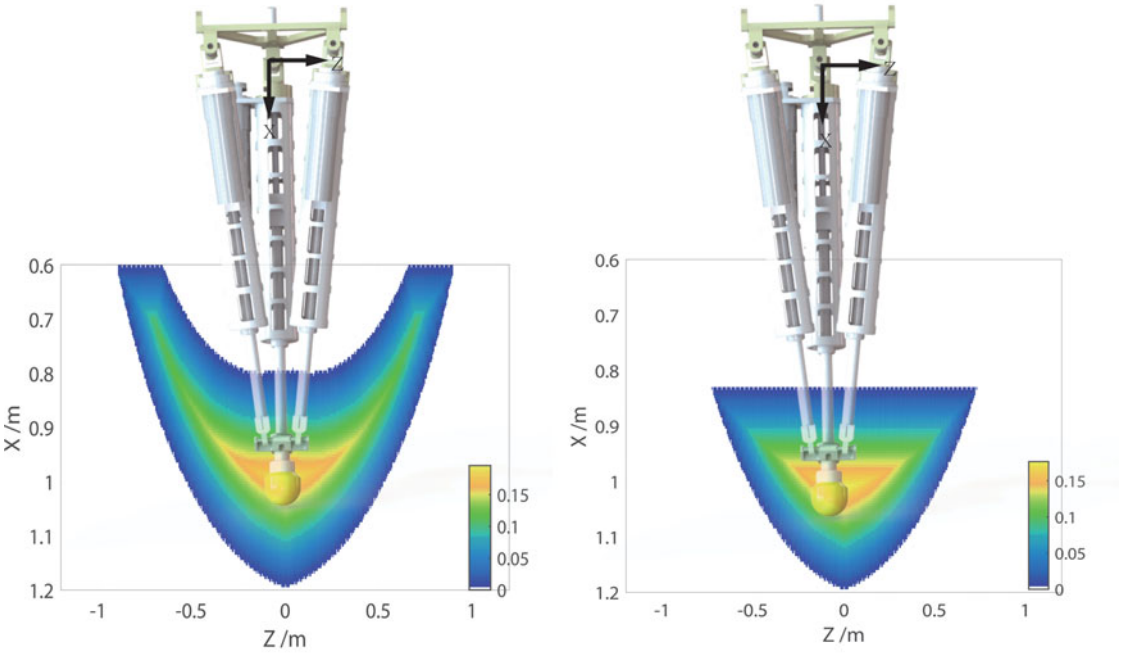

Fig. 4. Leg workspace and convex subspace viewed in the x-z plane w.r.t. the leg coordinate system.

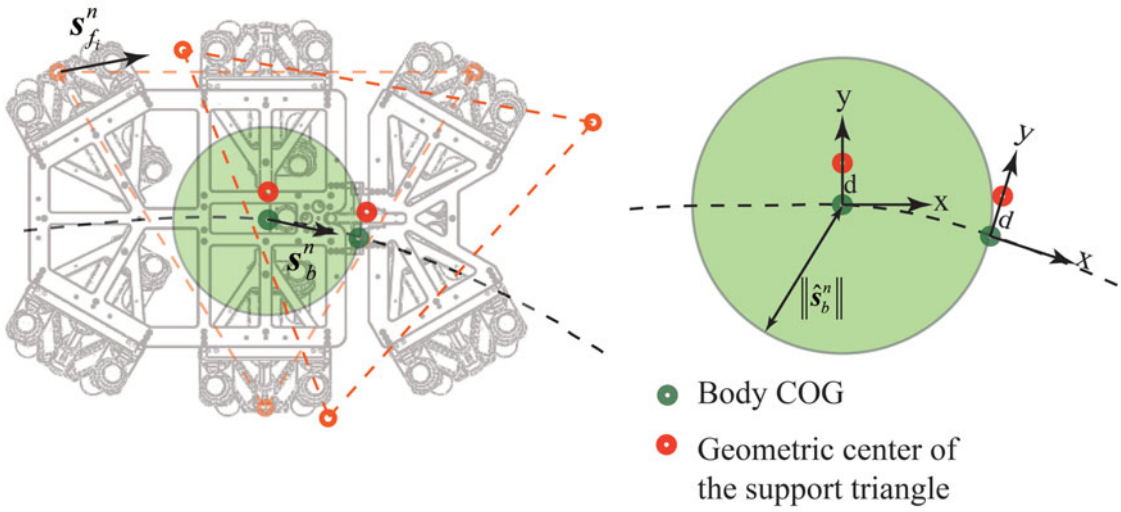

Fig. 5. Desirable triangle as searching centers for swing legs as the robot moves along its path.

the minimum distance of the foot tip to the boundary of the workspace (Fig. 4). In this paper, we employ the convex subset of the workspace for the convenience of convex optimization to be discussed in the next section. As illustrated, the convex subset only sacrifice the narrow workspace on the sides, which in our experience is little influential because they are hardly reached in walking tasks.

The RCMKM is given through the transformation of the leg configuration with maximum margin from the leg CS to the body CS and it is seen as the robot default standstill configuration. The desirable triangle of the three searching centers for swing legs corresponds to the three foot tip positions in RCMKM as the robot moves along its path (Fig. 5).

Referring to the computation ranges in the footstep cost, the foothold searching range should be sufficiently large to effectively avoid infeasible zones of the terrain, including edges, steer slopes and concave corners. Yet it can't be too large either, otherwise, leg kinematic deadlocks may occur.

https://doi.org/10.1017/S0263574717000418 Published online by Cambridge University Press

Table I. Searching range for footholds compared with cost computation range.

$[x_-, x_+, y_-, y_+]$	Foothold feasibility	Concave corner	Footholds search
x_-	$\lceil \frac{d_f}{r} \rceil$	$\lceil \frac{d_x}{r} \rceil$	$\lceil \frac{d_x}{2r} \rceil$
x_+	$\lceil \frac{d_f}{r} \rceil$	$\lceil \frac{d_x}{r} \rceil$	$\lceil \frac{d_x}{2r} \rceil$
y_-	$\lceil \frac{d_f}{r} \rceil$	$\lceil \frac{d_y}{r} \rceil$	$\lceil \frac{d_y}{2r} \rceil$
y_+	$\lceil \frac{d_f}{r} \rceil$	$\lceil \frac{d_y}{r} \rceil$	$\lceil \frac{d_y}{2r} \rceil$

According to Table I, the dimension parameters of the searching space are chosen as half of those of the concavity cost. The reason is that when the searching center is within the effective range of a nearby obstacle, such searching space is sufficient for the foothold to deviate from the most irregular terrain with a proper margin. For example, when a leg moves near a block, the proper searching range could lead the leg to either step to a certain distance before it or step onto it, effectively avoiding the concave corner.

An exhaustive search is applied in each step period to obtain the local minimum footstep cost position for a swing leg. It is efficient because the resolution of the grid map we applied is 2.5 cm and the number of terrain grid points to search is no more than one hundred for each swing leg. After choosing the suitable footholds, an optimization-based planning strategy based on the terrain description will be given for intermediate motion generation between two stances.

4. Optimized Configuration Planning

In this section, we will discuss on how to generate feasible and intermediate robot configurations in the constrained configuration space between two given stances. A fast and simple terrain description is proposed to obtain the minimum terrain information as the reference for swing legs. Constraints such as robot stability, kinematic reachability and collisions constraints are met by transforming the problem into a convex optimization problem. The solution gives feasible intermediate robot configurations, based on which, a simple trajectory of the robot is generated.

4.1. Local terrain reference

To cross over the terrain, a robot leg should be able to move referring to the form of the terrain. The terrain/obstacle reference generally involves an enveloping curve over the terrain. Such curves in most cases act as reference curves that the leg trajectory shall not reach within to avoid collisions. A box-shaped method was proposed by Kolter, *et al.*[22] in their earlier research. The box would simply envelope the whole terrain between two footholds and it was proved useful in certain terrains. Yet, for the robot that has a relatively smaller leg workspace, such method could increase the difficulty in terms of kinematics. A more refined reference trajectory with the convex hull approximation of the terrain has been widely applied by Kalakrishnan, *et al.*,[5] Belter and Skrzypczyński,[9] Ratliff, *et al.*[16] to describe the terrain reference from the start position to the goal position. Obviously, this method can accurately describe the terrain feature and is smoother. However, concerning the real-time factor and whole-body configuration planning on our robot, we suggest an intuitional description of the terrain as an alternative, with less waypoints and still functional.

We propose the Generalized Trapezoidal-Shaped Profile description of the local terrain (Fig. 6) between two neighboring footholds. Apart from the consideration of complexity, another reason why the trapezoidal terrain description is chosen is that we decompose the leg motion over the terrain into three phases, namely the ascent phase, the horizontal translation phase and the descent phase. The three-phased motion could in most cases cover any kind of terrain feature with relatively intuitional and fast generation and still utilize less demanding workspace than the box-shaped description. The terrain profile can be parametrically given as follow. A total of five parameters are involved (Table II), among which the clearance distance m is customer-defined. The parameters could be quickly obtained from the geometric feature of the terrain along the advancing plane. Referring to these parameters, the robot motion could then be purposefully optimized without further concerning other information of the terrain.

https://doi.org/10.1017/S0263574717000418 Published online by Cambridge University Press

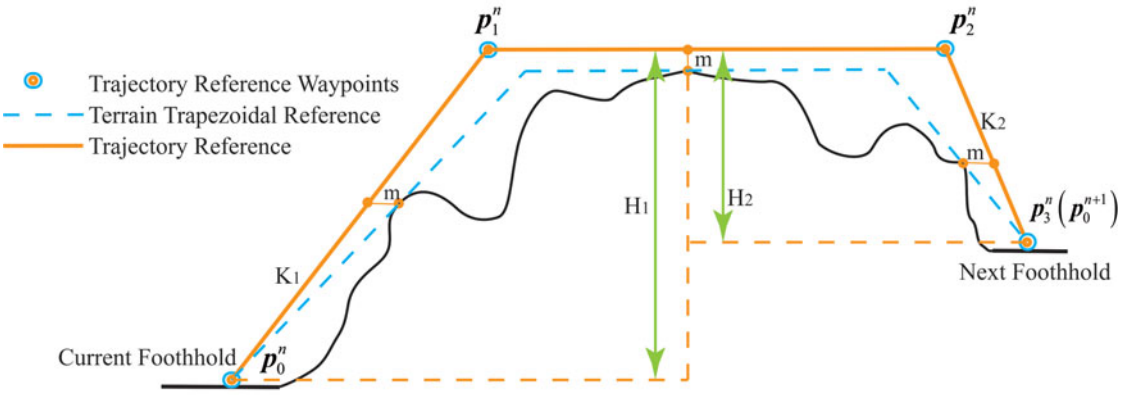

Fig. 6. The terrain reference is given as the blue-dashed lined derived from the three convex edge points of the terrain. The second segment of the terrain reference is horizontal, making the reference resemble a generalized trapezoidal form. The trajectory reference of the swing leg is obtained from the terrain reference with a clearance distance m to avoid foot tip collision with the terrain.

Table II. Terrain descriptive parameters.

Parameter	Representation
K1	The ascent gradient along the advancing plane.
K2	The descent gradient along the advancing plane.
H1	Leg ascending height.
H2	Leg descending height.
m	Clearance distance from the leg trajectory reference to the terrain reference

4.2. Featured configurations based on convex optimization

Once the footholds and the trajectory reference are obtained, the continuous motion of the robot could be investigated. Obviously, the overall robot motion is a series of configurations determined by the continuous variations of robot poses and all six legs positions. On flat terrains, it might be straightforward to separately plan the motion of each swing foot and the body. However, on irregular terrains, the continuous motion of the robot frequently meet limitations of the robot kinematics, collisions, etc. More precisely, it is imperative that,

(a) Each leg moves in a bounded workspace during the walking process.
(b) The body should be stable and not fall over.
(c) Any part of the robot except for foot tips should stay clear of the terrain.

These are strict physical constraints that if violated the robot can run into deadlocks, falling or collisions and can hardly accomplish the walking task. Inspired by the convex optimization formulation,[4,17] we suggest a method to fast generate whole-body configurations based on the waypoints of the three swing legs. Different from the above researches, the featured whole-body configurations between two stances are determined in one convex optimization problem. Like other convex optimization problem, the problem is formulized by problem variables, constraints and an objective. We will elaborate these in detail.

4.2.1. Problem variables. Referring to the trajectory waypoints of the swing legs, a total of n_{wp} waypoints of a swing leg are considered. In this case, n_{wp} equals to four due to the trapezoidal reference. Similarly, for the overall robot motion, we would also take into account four feasible configurations as featured configurations, among which $\boldsymbol{C}f_0^n$ and $\boldsymbol{C}f_3^n$ are stance configurations and the rest two $\boldsymbol{C}f_1^n$, $\boldsymbol{C}f_2^n$ are intermediate configurations with three swing legs in the air. A robot configuration is defined as:

$$\boldsymbol{C}f = \begin{pmatrix} \boldsymbol{p}_{f_1} & \boldsymbol{p}_{f_2} & \boldsymbol{p}_{f_3} & \boldsymbol{p}_{f_4} & \boldsymbol{p}_{f_5} & \boldsymbol{p}_{f_6} & \boldsymbol{p}_b & \boldsymbol{\psi}_b \end{pmatrix} \tag{15}$$

https://doi.org/10.1017/S0263574717000418 Published online by Cambridge University Press

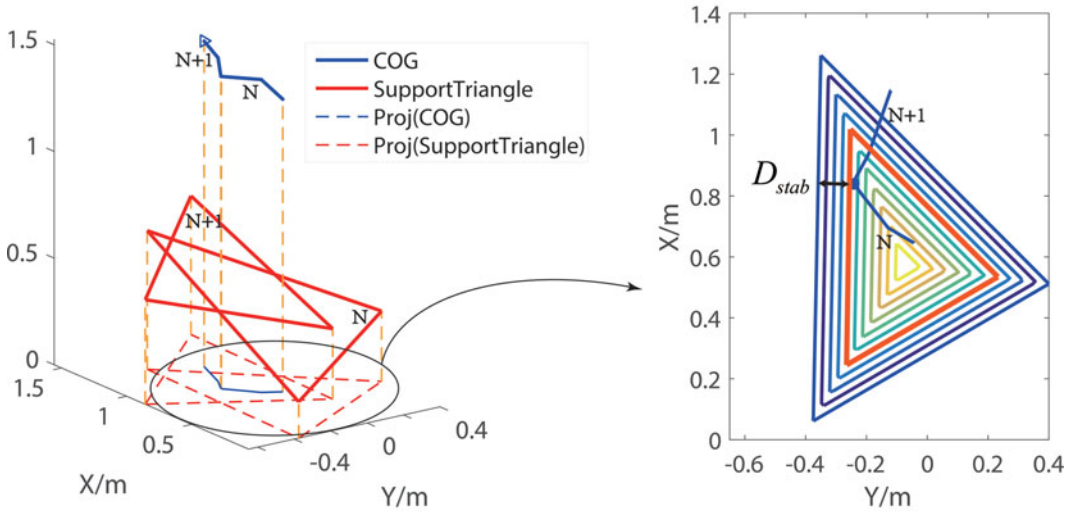

Fig. 7. Six-legged robot support triangle during Nth and N + 1th step. The COG projected trajectory should not violate the minimum stability margin D_{stab}.

The optimization-based approach aims to resolve the aforementioned configurations under mathematically formulated constraints. Problem variables are:

Discrete body poses: $(\boldsymbol{p}^n_{bj}, \boldsymbol{\psi}^n_{bj})$ for $j = 0, 1, 2, 3$.

Discrete foot tip positions: $\boldsymbol{p}^n_{f_i j}$ for $j = 0, 1, 2, 3,\ i \in swIDs$

It is worth mentioning that if the body orientation $\boldsymbol{\psi}_b$ is involved as the variable, then the convexity of the constrained variable space would be violated due to the computation of rotational transformation $R(\boldsymbol{\psi}_b)$, therefore the optimization problem is no more convex. We will first set the body rotation constant and investigate the motion in a convex subspace of the configuration space. We therefore modify the variables as:

Discrete body positions: $\boldsymbol{p}^n_{bj}$ for $j = 0, 1, 2, 3$.

Discrete foot tip positions: $\boldsymbol{p}^n_{f_i j}$ for $j = 0, 1, 2, 3, i \in swIDs$

In the end, an approach to integrate body rotation will be discussed.

4.2.2. Constraints and objective.

(a) Robot static stability

The six-legged robot introduced in this paper is a high payload robot whose motion tends to be static. The projection of the robot center of gravity (COG) to the horizontal plane should lies inside the projection of the support polygon formed by three stance legs to guarantee the static stability of the robot (Fig. 7). Also, an optimized adjustment of the robot COG could effectively avoid kinematic deadlocks of the leg if the terrain has considerable infeasible footholds.[23]

We term the stability margin as the minimum distance from the COG projection inside the triangle to the triangle edges projected on the horizontal plane. The margin could be computed through the intersection of three affine variable spaces representing distances to the edges (Fig. 7). Then the stability constraints could be expressed by the following convex inequalities.

$$\boldsymbol{p}_{\text{cog}} \in \Delta_{\text{stance}}(D_{\text{stab}}), \text{ for } \boldsymbol{p}_{\text{cog}} \in \left\{ \boldsymbol{p}^n_{\text{cog}0}, \boldsymbol{p}^n_{\text{cog}1}, \boldsymbol{p}^n_{\text{cog}2}, \boldsymbol{p}^n_{\text{cog}3} \right\} \tag{16}$$

in which $\Delta_{\text{stance}}(D_{\text{stab}})$ is the projected support triangle with the stability margin D_{stab} (0.125 m for our robot), and $\boldsymbol{p}_{\text{cog}}$ is the position of the robot COG. We reasonably assume that its position is a constant translational vector relative to the robot geometrical center $\boldsymbol{p}_b$ w.r.t. the robot body CS, because the robot walk quasi statically and with low speed. The walking period is around 6 s and the leg touchdown (TD) velocity is planned as zero. Moreover, the symmetric distribution of the light-weighted legs roughly cancels their contributions to the variation of the overall COG. In fact, small deviations may exist due to dynamics and other effects but could be compensated by the

https://doi.org/10.1017/S0263574717000418 Published online by Cambridge University Press

minimum margin D_{stab}. The orientation of the robot body is given by the IMU and it helps determine the orientation of the triangle of stance legs relative to the horizontal plane.

(b) Leg workspace

All six foot tips of the robot should be bounded by their respective workspace, especially for the leg in parallel mechanism, because the workspace is more limited than that of serial legs and is the direct reason of deadlocks. The problem is that for our robot, the three dimensional leg workspace is not convex. To formulize the problem, a convex subset of the workspace is applied. The convex subset is formed by the convex lower boundary determined by the maximum screw travel distance and an affine upper boundary in the leg coordinate frame (Fig. 4). All intermediate leg positions should be within the leg workspace:

$$^{L_i}\boldsymbol{p}_{f_i} \in {}^{L_i}WS_{\text{convex}},\ \text{for}\ {}^{L_i}\boldsymbol{p}_{f_i} \in \left\{{}^{L_i}\boldsymbol{p}^n_{f_i0}, {}^{L_i}\boldsymbol{p}^n_{f_i1}, {}^{L_i}\boldsymbol{p}^n_{f_i2}, {}^{L_i}\boldsymbol{p}^n_{f_i3}\right\},\ i = 1, 2, 3 \ldots 6 \tag{17}$$

The leg position $^{L_i}\boldsymbol{p}_{f_i}$ in the leg CS is computed from that in the ground reference CS by homogeneous transformation:

$$\begin{bmatrix} {}^{L_i}\boldsymbol{p}_{f_i} \\ 1 \end{bmatrix} = {}^{L_i}_{B}\boldsymbol{T} \begin{bmatrix} \boldsymbol{R}^{-1}\left(\boldsymbol{\psi}_b\right) \cdot \left({}^{G}\boldsymbol{p}_{f_i} - {}^{G}\boldsymbol{p}_b\right) \\ 1 \end{bmatrix} \tag{18}$$

where $^{L_i}_{B}\boldsymbol{T}$ is constant. It is easy to observe that if the robot orientation $\boldsymbol{\psi}_b$ is set to be constant, then the function becomes an affine transformation of the position variables $\boldsymbol{p}_{f_i}$ and $\boldsymbol{p}_b$.

(c) Collisions

The collisions discussed here is in fact the collisions between robot parts and the environment, more specifically, the shin contact, because the robot body can hardly impact the ground due to its considerable elevation and leg–leg interferences are effectively avoided due to limited step length. We investigate the shin-terrain collision by modeling the robot leg configuration (*LCf*) as a convex polyhedral computed from translational variables of body and legs. In that way, for one leg configuration, the collision-free between each vertex of the polyhedral and terrain could guarantee the clearance of the whole leg and terrain. As for a series of sequential leg configurations, we expect that any affine combination of the two neighboring configurations is identically constrained thus forming a feasible robot configuration connection in space. Therefore, it is required that each of the two neighboring configuration share a common convex constraint space determined by the terrain trapezoidal reference (Fig. 8).

$$LCf_0, LCf_1 \in C_1 \tag{19}$$

$$LCf_1, LCf_2 \in C_2 \tag{20}$$

$$LCf_2, LCf_3 \in C_3 \tag{21}$$

Table III indicates the system variables and the commonly constrained configurations. It should be noted that stability constraints and workspace constraints are identical w.r.t. different configurations. Only the collision constraint involves different constraint spaces according to the terrain feature (in our case C_1 , C_2 and C_3).

(a) Objective

If all the above constraints should be met, then the robot is able to steadily cross over the terrain without deadlocks or collisions, applying a polyline trajectory connecting featured configurations. As for the objective, we consider it as the energy cost of the robot motion in the task space, which comprises the body task space and the leg task space.

$$J_{\text{obj}} = \omega_{\text{body}} \sum\nolimits_{j=0}^{2} \left\| \boldsymbol{p}^n_{bj} - \boldsymbol{p}^n_{b(j+1)} \right\|^2 + \omega_{\text{leg}} \sum\nolimits_{i=1}^{6} \sum\nolimits_{j=0}^{2} \left\| \boldsymbol{p}^n_{f_ij} - \boldsymbol{p}^n_{f_i(j+1)} \right\|^2 \tag{22}$$

https://doi.org/10.1017/S0263574717000418 Published online by Cambridge University Press

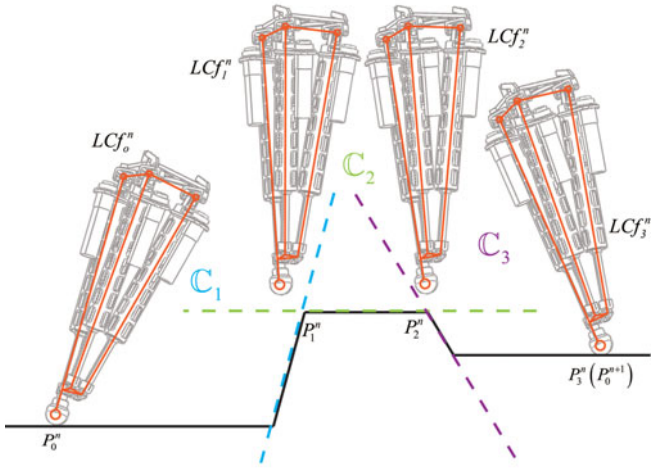

Fig. 8. Consecutive leg configurations when crossing over an obstacle and corresponding constraint spaces.

Table III. The overall problem constraints, constraint type w.r.t. variables and configurations involved.

Constraints	Type	Configurations
$p_{\text{cog}\,j} \in \Delta_{\text{stance}}(D_{\text{stab}})$, for $j = 0, 1$	Affine	$C f_0$, $C f_1$,
${}^{L_i}p_{f_i j} \in {}^{L_i}WS_{\text{convex}}$, for $j = 0, 1$ and $i = 1 \sim 6$	Convex	
$LC f_{i0}, LC f_{i1} \in C_{i1}$ for $i = 1 \sim 6$	Affine	
$p_{\text{cog}\,j} \in \Delta_{\text{stance}}(D_{\text{stab}})$, for $j = 1, 2$	Affine	$C f_1$, $C f_2$
${}^{L_i}p_{f_i j} \in {}^{L_i}WS_{\text{convex}}$, for $j = 1, 2$ and $i = 1 \sim 6$	Convex	
$LC f_{i1}, LC f_{i2} \in C_{i2}$ for $i = 1 \sim 6$	Affine	
$p_{\text{cog}\,j} \in \Delta_{\text{stance}}(D_{\text{stab}})$, for $j = 2, 3$	Affine	$C f_2$, $C f_3$
${}^{L_i}p_{f_i j} \in {}^{L_i}WS_{\text{convex}}$, for $j = 2, 3$ and $i = 1 \sim 6$	Convex	
$LC f_{i2}, LC f_{i3} \in C_{i3}$ for $i = 1 \sim 6$	Affine	

in which ω_{body} and ω_{leg} are weights of different objectives. We assign $\omega_{\text{body}} = 10\omega_{\text{leg}}$ to achieve a less abrupt motion of the robot body.

We therefore minimize the objective function J_{obj} as a quadratic objective of problem variables. The overall motion optimization is formulized into a conic optimization problem. It is efficient to solve the problem applying the off the shelf software.

Given the feasible configurations of the robot, any affine combination of the neighboring configurations is in the constrained configuration space. Out of this consideration, a simple three-segmented trajectory of the leg w.r.t. the ground CS is employed, namely the ascending segment, the horizontal segment and the descending segment. Each of the segments are assured with three-dimensional linearity in space applying a simple sinusoid-based interpolation that also guarantees the zero velocity in the beginning and ending of the segment.

$$ {}^{G}\boldsymbol{p}_{f_i}(t) = \frac{1+\cos(s_k)}{2}\,{}^{G}\boldsymbol{p}^{n}_{f_i(k-1)} + \frac{1-\cos(s_k)}{2}\,{}^{G}\boldsymbol{p}^{n}_{f_i k} \tag{23} $$

with $s_k = \frac{t}{T_k}\pi$, $t \in [0, T_k]$, $k = 1, 2, 3$.

4.3. Integration of body rotation

The proposed convex problem formulation could resolve obstacle traversing in a strict and continuous sense with fixed body orientation. Yet, for more hazardous terrains, the robot should alter its orientation to better adapt to the inclination of the terrain. Generally, for a six-legged robot, the robot body is dexterous and the end effector pose (body pose) has infinite solutions if the positions of all six legs are given. Due to the dexterity of the robot body and non-convexity if the rotational variables are involved, we suggest to roughly provide the robot with optimally estimated orientation and solve the

https://doi.org/10.1017/S0263574717000418 Published online by Cambridge University Press

Table IV. Simulation parameters in ADAMS.

Parameter	Value
Gravity	9.8N/Kg
Integrator	GSTIFF
Step size	0.1s
Restitution coefficient	0.5
Friction force type	Coulomb
Static friction coefficient	0.8
Dynamic friction coefficient	0.5

body translational movements through the strict convex optimization using the planning scheme of the previous section.

Deits and Tedrake[4] proposed the linear approximation of sinusoid functions to include the yaw angle as a variable into the convex optimization. However, the constraints discussed were different from what we formulized and doing so would still violate the convexity of the problem. However, for large and heavy robots like the one discussed in this paper, we reasonably suppose that in most situations when they walk on traversable terrains, the orientation variation during one single step is rather small. We therefore approximate the continuous body orientation with linearly monotonic interpolation of the beginning and ending orientation of the robot. The linear interpolation is w.r.t. the yaw-pitch-roll Euler angle space to describe the body orientation, which works just fine for small rotations.

$$ {}^{G}\boldsymbol{\psi}_b(t) = \frac{1+\cos\left(\frac{t}{T}\pi\right)}{2}\,{}^{G}\boldsymbol{\psi}_b^{n} + \frac{1-\cos\left(\frac{t}{T}\pi\right)}{2}\,{}^{G}\boldsymbol{\psi}_b^{n+1} \tag{24} $$

To compute the optimal body orientation in the goal configuration, the singular value decomposition (SVD) method is applied to find an optimal transformation matrix of the body w.r.t. the ground CS when all legs are in their stance phase. The optimality discussed here is the least square based optimality w.r.t. the leg kinematic margin.

Foot tip positions with largest kinematic margin w.r.t. the body CS ${}^{B}\tilde{\boldsymbol{p}}_{f_i}$ is firstly given referring to RCMKM. Then, we look for an optimal transformation $\tilde{\boldsymbol{\psi}}_b$ and $\tilde{\boldsymbol{p}}_b$ of the robot body w.r.t. the ground, such that:

$$ \left(\tilde{\boldsymbol{\psi}}_b, \tilde{\boldsymbol{p}}_b\right) = \mathrm{argmin}_{\boldsymbol{\psi}_b, \boldsymbol{p}_b} \sum_{i=1}^{6} w_i \left\| R\left(\boldsymbol{\psi}_b\right) \cdot {}^{B}\tilde{\boldsymbol{p}}_{f_i} + \boldsymbol{p}_b - {}^{G}\boldsymbol{p}_{f_i} \right\|^2 \tag{25} $$

Referring to Sorkine,[24] the weighted centroids of ${}^{B}\tilde{\boldsymbol{p}}_{f_i}$ and ${}^{G}\boldsymbol{p}_{f_i}$ are:

$$ {}^{B}\bar{\boldsymbol{p}}_f = \frac{\sum_{i=1}^{6} w_i\, {}^{B}\tilde{\boldsymbol{p}}_{f_i}}{\sum_{i=1}^{6} w_i} \tag{26} $$

$$ {}^{G}\bar{\boldsymbol{p}}_f = \frac{\sum_{i=1}^{6} w_i\, {}^{G}\boldsymbol{p}_{f_i}}{\sum_{i=1}^{6} w_i} \tag{27} $$

And the optimal rotation is

$$ R\left(\tilde{\boldsymbol{\psi}}_b\right) = \boldsymbol{V} \begin{pmatrix} 1 & & \\ & 1 & \\ & & \ddots \\ & & & \det\left(\boldsymbol{V}\boldsymbol{U}^{\boldsymbol{T}}\right) \end{pmatrix} \boldsymbol{U}^{\boldsymbol{T}} $$

https://doi.org/10.1017/S0263574717000418 Published online by Cambridge University Press

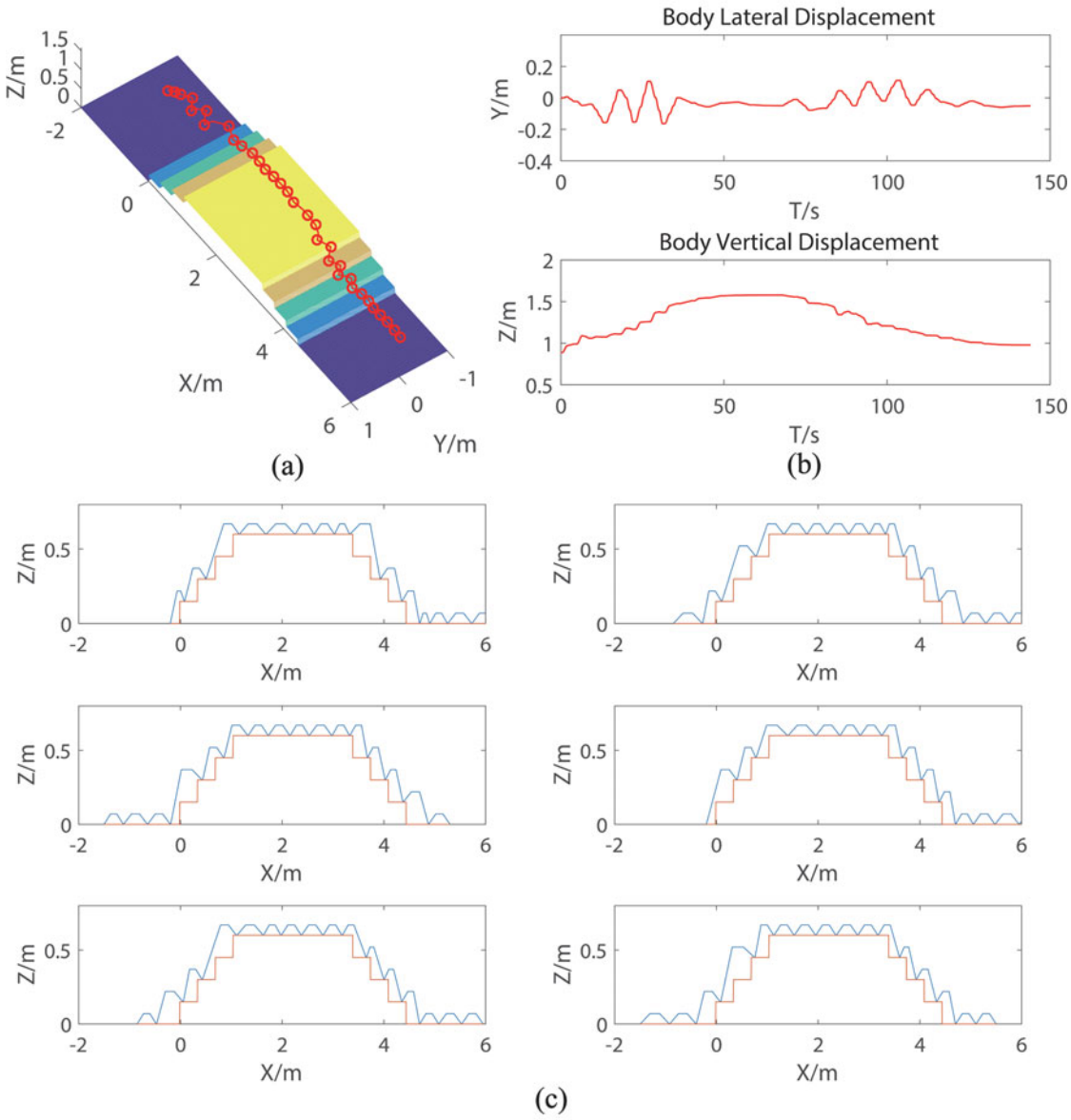

Fig. 9. Body COG and leg trajectories on clustered obstacles with the elevation scaled from 0.1 m to 0.2 m. (a) Body COG 3D trajectory. (b) The evolution of body lateral and vertical displacements. (c) Legs trajectories lateral view.

where $\boldsymbol{U}$ and $\boldsymbol{V}$ are derived from the SVD of the covariance matrix $\boldsymbol{S}$ between ${}^{B}\tilde{\boldsymbol{p}}_{f}$ and ${}^{B}\boldsymbol{p}_{f}$, with $\boldsymbol{S} = \boldsymbol{U}\Sigma\boldsymbol{V}^{T}$.

Respectively, constraints should also be modified. In Section 4.2, all constraints involving the robot orientation take the same constant value. We simply pose an additional constraint on each intermediate configurations with both of the starting and ending robot orientation. Therefore, the feasible space of intermediate configurations is the overlapped feasible space of two different orientations.

Due to such adjustment of the problem to involve the robot rotation, the violation of the robot constraints is limited to a very small extent. However, these violations can be compensated by employing slightly larger collision clearance and the minimum kinematic margin in the workspace.

5. Simulation and Experiments

Simulations and experiments were carried out on a set of irregular terrains. For the simulation, we used MATLAB for the optimization algorithm to generate robot trajectories and applied the

https://doi.org/10.1017/S0263574717000418 Published online by Cambridge University Press

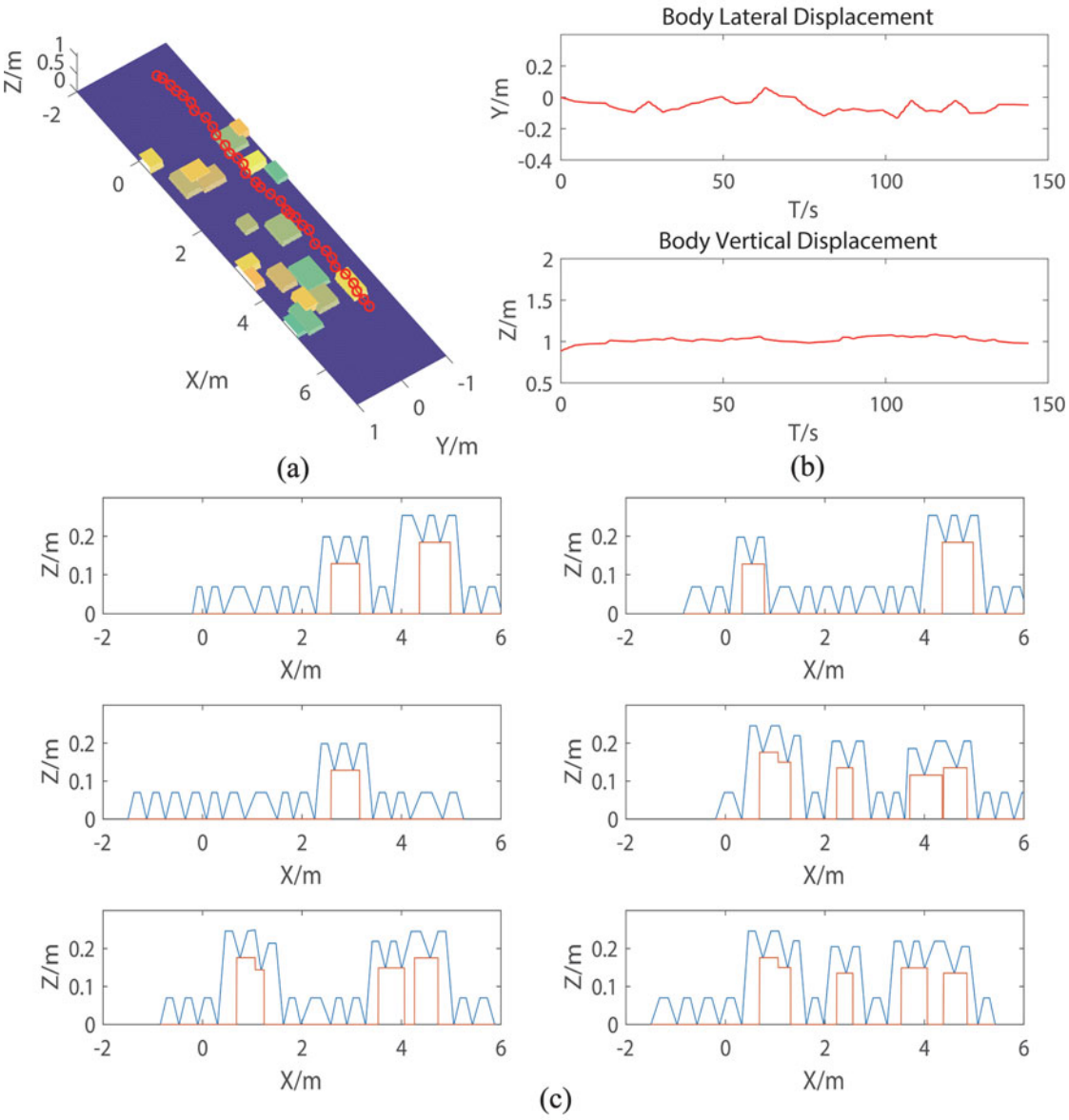

Fig. 10. Body COG and leg trajectories on staircases of 0.15 m × 0.35 m. (a) Body COG 3D trajectory. (b) The evolution of body lateral and vertical displacements. (c) Legs trajectories lateral view.

screw trajectories as inputs into the multi-body dynamics simulation environment. The simulation parameters are shown in Table IV. The rubber foot tips offer sufficiently large friction coefficients. Figures 9 and 10 illustrate robot motions on terrains with clustered obstacles and on a series of staircases. The trajectory of each leg effectively steer clear of the terrain obstacles. Each trajectory is the concatenation of a series of local leg trajectories referring to the terrain feature. The lateral and vertical body displacements are also given. The degree of the body lateral motion increases when the terrain becomes more irregular, for example, when the robot is walking over stairs (Fig. 10).

Field tests (Fig. 11) on the robot gave satisfying results. We set the robot step period to 6 s to avoid potential dynamic instability of the robot body. The robot was able to successfully traverse terrains without deadlock (Fig. 12) or collisions. The stability margin always stayed larger than the planned minimum D_{stab} (Fig. 13). However, motion inaccuracy was observed, which derives from the difference between the experiment and the simulation. First, the terrain elevation map had an elevation error of less than 2 cm for each grid point. Second, the robot mechanical system also has kinematic errors which can't be eliminated. These experimental factors lead to the inconsistent TD

https://doi.org/10.1017/S0263574717000418 Published online by Cambridge University Press

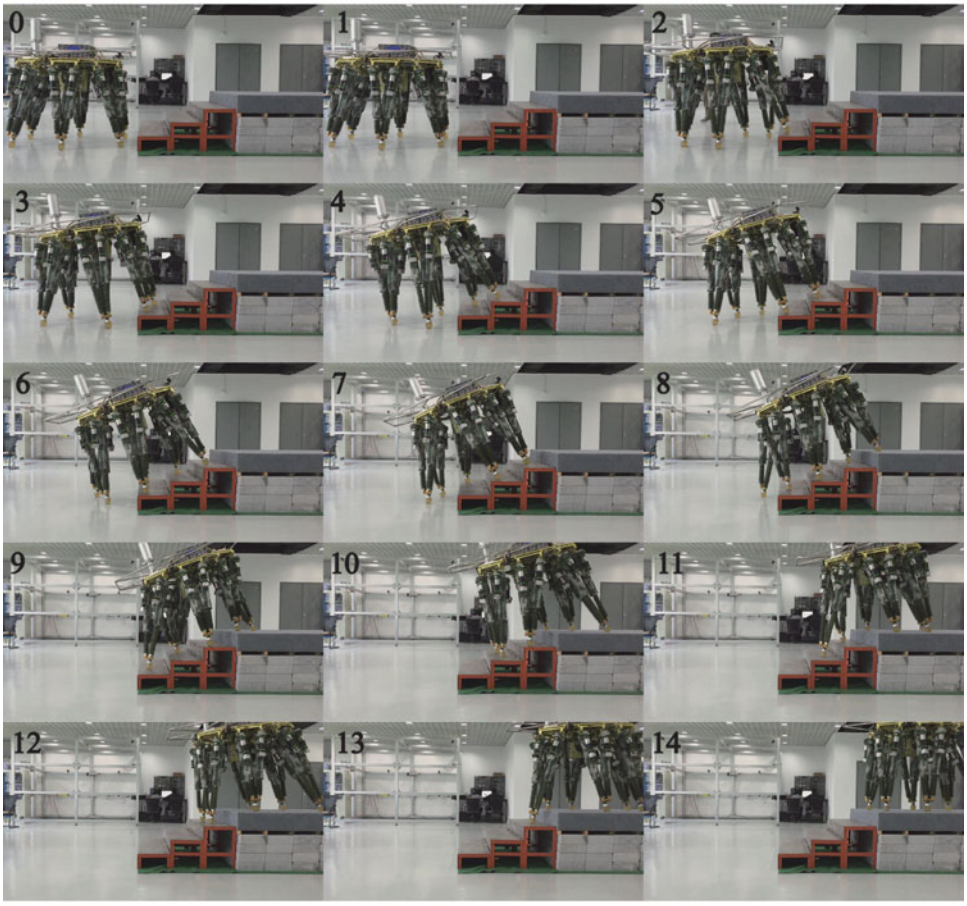

Fig. 11. Snapshots of the six-legged robot walking over staircases.

between the swing legs and the ground, as well as small errors of the advancing distance and the body attitude during each foot step.

The vision error could be compensated by a physical TD signal. We employed the indirect force estimation method to roughly examine the TD of each swing leg when the support force is big enough.[25] If the swing leg tracking the planned trajectory does not touch down, we would reschedule the trajectory and extend the leg. Otherwise, if TD is physically detected, we would decelerate the moving leg with the maximum deceleration until it stops to zero velocity. The current walking step will terminate until all three swing legs reach zero velocity. The TD mechanism guarantees reliable foot support and compensate the error between the visionary terrain and the physical terrain. Upon TD, we record the motor inputs of the robot as well as the IMU orientation as the robot configuration information for the optimized planning of the next step. As for the second factor, the leg kinematic error which is less than 5 mm is rather small thanks to the accuracy of the parallel mechanism. It is tolerable for the constraints since we've set sufficient stability and collision margins for the planner to take into account potential errors. Therefore, in real-world applications, the robot could still realize motions with reliable leg support and without violating constraints. As long as these two terms are satisfied, the walking task is executable. For the longtime term consideration, the robot motion in real world and in the simulation may gradually diverge from each other due to the aforementioned motion error. However, this is the non-eliminable effect caused by the system and accumulated independently from numerous steps, not caused by the planning algorithm. The planning algorithm was validated both in the simulation and in the experiment.

As for software implementation, we employed the Mosek optimization software[26] as the convex optimization solver for implementation. The motion planning problem was formulized into a conic optimization problem which could be resolved around several milliseconds. The overall computation

https://doi.org/10.1017/S0263574717000418 Published online by Cambridge University Press

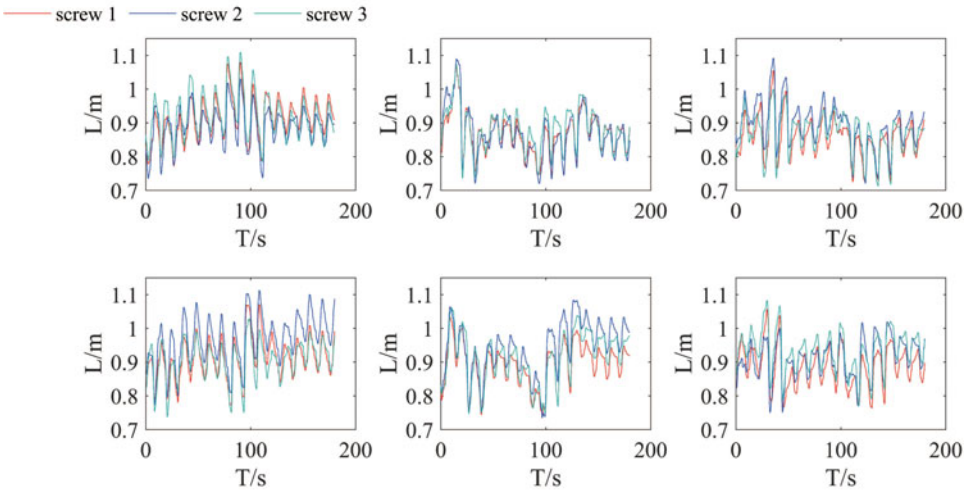

Fig. 12. Screw inputs of each leg during walking stairs. The computed screw inputs stayed bounded as required ($0.691\ \text{m} < L_1 < 1.091\ \text{m}$ and $0.713\ \text{m} < L_2, L_3 < 1.112\ \text{m}$) even if the body rotation is involved.

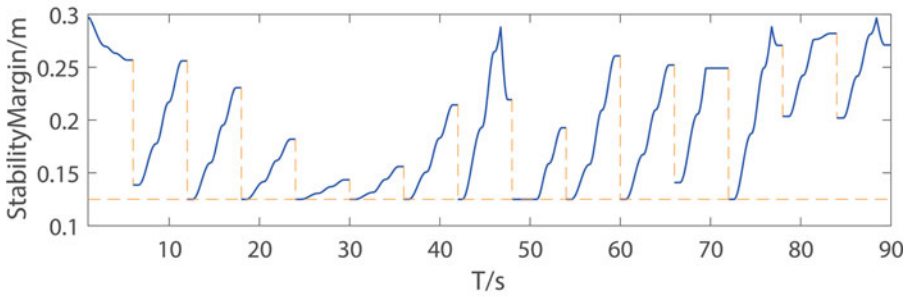

Fig. 13. The evolution of the robot stability margin during walking. The margin stays larger than the given value of 0.125 m. The sudden jump of the margin is due to the switch of the support legs.

time for each step including the terrain modeling was around 0.1 s in another thread apart from the real-time motor servo thread. As a matter of fact, this is quite satisfying for the robust motion generation on irregular terrains, especially when terrain information is not preoccupied offline before the locomotion task starts. Our two-step fast motion planning was proved effective.

6. Conclusion

This paper proposed a two-step planner for a six-legged robot walking on irregular terrains. The planner is a whole-body and whole-step planner, therefore during planning, leg mobility, terrain features and body steadiness are all considered in a structured scheme. Both terrain modeling and motion generation were efficiently carried out, via concise terrain description and the convex optimization formulation. The fast generation of motions defined by featured configurations is intuitive and efficient. In addition, the planned motion of the robot could adapt to the irregular terrain autonomously without offline precomputation. At the same time, static stability, collision free and leg workspace constraints were equally satisfied. Off the shelf software made the planner possible for implementation on our robot, our approach was proved to be effective.

Future research consists of more aggressive locomotion of the six-legged robot. Dynamic behaviors of the legs and the body will be investigated to achieve dynamically stable, smoother and faster motions. Continuous force identification and load estimation using force sensors would also be involved in our future research to gain a better dynamic response to the outside environment.

https://doi.org/10.1017/S0263574717000418 Published online by Cambridge University Press

Acknowledgments
This study was partially supported by the National Natural Science Foundation of China (No.U1613208) and the National Basic Research Program of China (973 Program) (No. 2013CB035501)

Supplementary material
To view supplementary material for this article, please visit https://dx.doi.org/10.1017/S0263574717000418.

References

1. U. Saranli, M. Buehler and D. E. Koditschek, "RHex: A simple and highly mobile hexapod robot," *Int. J. Robot. Res.* **20**, 616–631 (2001).
2. J. J. Kuffner Jr, K. Nishiwaki, S. Kagami, M. Inaba and H. Inoue, "Footstep Planning Among Obstacles for Biped Robots," Proceedings of the Intelligent Robots and Systems, 2001, IEEE/RSJ International Conference on, (Maui, Hawaii, USA, 2001) pp. 500–505.
3. Y. Ayaz, K. Munawar, M. B. Malik, A. Konno and M. Uchiyama, "Human-like approach to footstep planning among obstacles for humanoid robots," *Int. J. Humanoid Robot.* **4**, 125–149 (2007).
4. R. Deits and R. Tedrake, "Footstep Planning on Uneven Terrain with Mixed-integer Convex Optimization," *Proceedings of the* Humanoid Robots (Humanoids), 2014 14th IEEE-RAS International Conference on, (Madrid, Spain, 2014) pp. 279–286.
5. M. Kalakrishnan, J. Buchli, P. Pastor, M. Mistry and S. Schaal, "Learning, planning, and control for quadruped locomotion over challenging terrain," *Int. J. Robot. Res.* **30**, 236–258 (2011).
6. M. Zucker et al., "Optimization and learning for rough terrain legged locomotion," *Int. J. Robot. Res.* **30**, 175–191 (2011).
7. J. Z. Kolter and A. Y. Ng, "The stanford littledog: A learning and rapid replanning approach to quadruped locomotion," *Int. J. Robot. Res.* **30**, 150–174 (2011).
8. F. Ozguner, S. Tsai and R. McGhee, "An approach to the use of terrain-preview information in rough-terrain locomotion by a hexapod walking machine," *Int. J. Robot. Res.* **3**, 134–146 (1984).
9. D. Belter and P. Skrzypczyński, "Rough terrain mapping and classification for foothold selection in a walking robot," *J. Field Robot.* **28**, 497–528 (2011).
10. D. Belter, "Optimization-based approach for motion planning of a robot walking on rough terrain," *J. Autom. Mobile Robot. Intell. Syst.* **7**, 34–41 (2013).
11. D. Belter and P. Skrzypczyński, "Posture Optimization Strategy for a Statically Stable Robot Traversing Rough Terrain," *Proceedings of the* Intelligent Robots and Systems (IROS), 2012 IEEE/RSJ International Conference on, (Vilamoura, Algarve, Portugal, 2012) pp. 2204–2209.
12. E. Masehian and D. Sedighizadeh, "Classic and heuristic approaches in robot motion planning-a chronological review," *World Acad. Sci., Eng. Technol.* **23**, 101–106 (2007).
13. L. E. Kavraki, P. Švestka, J.-C. Latombe and M. H. Overmars, "Probabilistic roadmaps for path planning in high-dimensional configuration spaces," *IEEE Trans. Robot. Autom.* **12**, 566–580 (1996).
14. J. J. Kuffner and S. M. LaValle, "RRT-connect: An Efficient Approach to Single-query Path Planning," *Proceedings of the* Robotics and Automation, 2000. Proceedings. ICRA'00. IEEE International Conference on, (San Francisco, CA, USA, 2000) pp. 995–1001.
15. K. Hauser, T. Bretl, J.-C. Latombe, K. Harada, and B. Wilcox, "Motion planning for legged robots on varied terrain," *Int. J. Robot. Res.* **27**, 1325–1349 (2008).
16. N. Ratliff, M. Zucker, J. A. Bagnell and S. Srinivasa, "CHOMP: Gradient Optimization Techniques for Efficient Motion Planning," *Proceedings of the* Robotics and Automation, 2009. ICRA'09. IEEE International Conference on, (Kobe, Japan, 2009) pp. 489–494.
17. J. Z. Kolter and A. Y. Ng, "Task-Space Trajectories Via Cubic Spline Optimization," in *Proceedings of the* Robotics and Automation, 2009. ICRA'09. IEEE International Conference on, (2009) pp. 1675–1682.
18. Y. Pan and F. Gao, "A new 6-parallel-legged walking robot for drilling holes on the fuselage," *Proc. Institution Mech. Eng., C: J. Mech. Eng. Sci.ence*, **228**(4), 753–764 (2013).
19. H. Du and F. Gao, "Fault tolerance properties and motion planning of a six-legged robot with multiple faults," *Robotica* FirstView, 1–18 (2016).
20. J.-P. Merlet, Parallel *Robots*, vol. 74, (Springer Science & Business Media, PO Box 17, 3300 AA Dordrecht, The Netherlands, 2012).
21. D. Belter, P. Labecki and P. Skrzypczyński, "Map-based Adaptive Foothold Planning for Unstructured Terrain Walking," *Proceedings of the* Robotics and Automation (ICRA), 2010 IEEE International Conference on, (Anchorage, Alaska, USA, 2010) pp. 5256–5261.
22. J. Z. Kolter, M. P. Rodgers and A. Y. Ng, "A Control Architecture for Quadruped Locomotion Over Rough Terrain," Proceedings of the - IEEE International Conference on Robotics and Automation, (Pasadena, CA, USA, 2008) pp. 811–818.

23. W. Chen, K. H. Low and S. H. Yeo, "Adaptive gait planning for multi-legged robots with an adjustment of center-of-gravity," *Robotica* **17** 391–403 (1999).
24. O. Sorkine, "Least-squares rigid motion using svd," *Technical Notes* **120**, 3 (2009).
25. Y. Xu, F. Gao, Y. Pan and X. Chai, "Method for six-legged robot stepping on obstacles by indirect force estimation," *Chinese J. Mech. Eng.* 1–11 (2016).
26. M. Aps. The MOSEK optimization software. Available: https://mosek.com/

https://doi.org/10.1017/S0263574717000418 Published online by Cambridge University Press